The Journal of the Astronautical Sciences (2019) 66:46–67
https://doi.org/10.1007/s40295-019-00154-7

Spacecraft Electrostatic Force and Torque Expansions Yielding Appropriate Fidelity Measures

Joseph Hughes[1] · **Hanspeter Schaub**[2]

Published online: 10 May 2019

Abstract

Charged spacecraft experience electrostatic forces and torques from both charged neighboring spacecraft and the local space environment. These forces and torques can be used for a variety of novel touchless actuation concepts. In contrast to the multipole method which provides an expansion of the potential field, this paper presents a direct binomial series expansion of the forces and torques called the Appropriate Fidelity Measures (AFMs) method. A two-stage process is presented where first the force and torque vectors are expanded assuming a known charge distribution, followed by a second stage which provides an approximation of the charge distribution through the susceptibilities of the measures. AFMs provide a direct analytical solution and thus provide new insight for charged single- and two-body configurations. The accuracy of a truncated expansion is numerically studied and validated. With a second-order AFM solution, the errors drop below 5% at separations greater than ~ 6 craft diameters. This new method is well-suited for control analysis due to the analytical solutions produced. An AFM solution of the torque on an axis-symmetric cylinder is developed that yields closed form analytic solutions that match prior numerically fit solutions.

Keywords Electrostatics · Touchless Actuation · Space Debris

Introduction

In the Geosynchronous Earth Orbit (GEO) regime, satellites charge to very high voltages on the order of tens of kiloVolts [9]. This charging causes small forces and

✉ Joseph Hughes
joseph.hughes@colorado.edu

Hanspeter Schaub
hanspeter.schaub@colorado.edu

[1] 275 ECEE, 431 UCB, University of Colorado Boulder, Boulder, CO 80309, USA

[2] 321 ECNT, 431 UCB, University of Colorado Boulder, Boulder, CO 80309, USA

torques on the body due to interactions with Earth's magnetic field. This can change the orbits of uncontrolled lightweight debris objects [10, 21, 22, 30]. If nearby spacecraft use active charging such as through electron and ion guns, larger forces and torques are felt between the crafts. This enables novel Coulomb formation flying missions [7, 16, 23, 26, 27]. Electrostatic forces are also being studied for touchless re-orbiting of GEO debris to a graveyard orbit in a matter of months using the Electrostatic Tractor (ET) [2, 33]. The ET concept directs the charge emission of the servicer or tug at the debris object to yield an attractive inter-spacecraft force. If a spacecraft has a non-spherical shape, it may also experience torques which can be harnessed for touchless de-spin before servicing or grappling [3, 5, 6].

There are many separate challenges to electrostatic actuation such as prescribing the appropriate electron and/or ion beam current and voltage, sensing the voltage, position, and attitude of a passive space object, and designing control laws that perform well for either tugging or de-spinning. This paper addresses the challenge of analytically predicting the force and torque vectors on each spacecraft given the voltages of each craft, and their relative position and attitude. This is important to perform dynamic stability and control analysis, as well as implement robust feedback control solutions. For example, Reference [17] illustrates how an under-prediction of the nominal ET force can lead to an unstable bifurcation in the closed loop dynamics.

The problem of two charged conductors interacting through electrostatics is similar to that of two bodies interacting gravitationally. The differential force in both cases is proportional to the product of either the masses or charges, and inversely proportional to the square of the distance between them. The gravitational problem can be readily solved using conic sections if both bodies are treated as point masses. For added fidelity, the larger body is treated as a general shape through the use of a spherical harmonic expansion. If both bodies are near the same size and very close, they must both be treated in a general manner solving the full gravitational two-body problem. This problem can be solved using a range of methods including expansions of mass distribution through MacCullagh's approximation [13], inertia integrals [18] or numerically using a lumped-mass approach [34]. In the electrostatic problem, there is also an added complication: the total mass and its distribution is fixed in a rigid body while the total charge and associated charge distribution change easily within a conductor. As the two conductors rotate and translate, the charge distribution changes and impacts the electrostatic forces and torques. For example, consider two negatively charged objects approaching each other. The electrons will repel each other and gather on the far sides of the objects, causing a differential charge distribution. In contrast, as two rigid asteroids approach each other their mass distribution remain unchanged.

Many methods exist to solve the electrostatic problem numerically, and they all begin with prediction of the charge distribution. This can be done using full FEA software which is very accurate but much too slow for dynamics simulations, or more faster methods like the Method of Moments [12, 15]. Once the charge distribution is known, the total Coulomb force can be found by summing the force between every facet in one body and every facet in the other body. A new method for force and torque prediction is the Multi-Sphere Method (MSM) [37], which places spheres of tunable radii and position throughout the conductor. This process divides into Surface

MSM (SMSM), which was optimized for large numbers of spheres constrained to be on the surface of the conductor by Stevenson et. al. in [38] and Volume MSM (VMSM), which uses a small number of spheres with unconstrained positions and was optimized by Chow et. al. in [8] and later using E field matching by Ingram et al. in [24]. While these methods offer an excellent trade study between accuracy and speed, all are numerical and do not enable closed-form analysis. Analytical insight is instrumental in any dynamics and stability studies, such as for the de-spin and ET concept.

Analytical formula for the electrostatic two-body problem are found for the special case of two conducting spheres using the Method of Images [25, 28, 29]. If the bodies are not spherical, the multipole expansion method can be used to find the electric potential in the vicinity of a charge distribution by expanding the charge distribution in powers of $1/R$ [25]. The potential energy of two charged molecules can also be found and differentiated with respect to position attitude to find force and torque [31]. These expansions use terms similar to the inertia integrals used by Hou [18]. The conference paper cited in Reference [19] introduces a similar method for finding the electrostatic force and torque between two charged spacecraft, but differs in that it does not find the potential but finds the force and torque directly. This method for predicting force and torque is called the Appropriate Fidelity Measures (AFM) method, named for the measures of the charge distribution that appear due to the appropriate fidelity truncation of the binomial series.

Reference [19] illustrates an early form of the AFM concept and investigates some special cases of an isolated body in a flat or radial field, but doesn't develop the full two body AFM theory. Flat field analysis was furthered for the special case of a High Area-to-Mass Ratio (HAMR) object's orbit being perturbed by Earth's magnetic field in References [21, 22]. This paper provides the first comprehensive theory of AFMs for general spacecraft applications, including the general case of two interacting charged bodies, and shows how the radial field is a special case of the general two body problem. Providing this general framework allows modeling a range of scenarios including locally flat environmental fields as well as Coulomb forces using the same equations. This work differs from the multipole expansion cited in Reference [31] in that this work also presents a method for predicting the moments of the charge distribution from the voltage and attitude of each craft as well as their separation.

The general AFM formulation is developed by first investigating the field integrals over both bodies of general shape. These integrals are approximated using a binomial series which is truncated at the point corresponding to appropriate fidelity for the scenario. Three key moments of the charge distribution appear when solving these integrals, which allow for compact representation of the force and torque. The second step is to predict these moments from parameters more easily accessed in situ such as the voltage of each craft, the relative attitude of the crafts, and their separation. In the case of an isolated object the ambient magnetic and electric fields are used along with the object's voltage. The charge distribution is evaluated for general shapes, potentials and external magnetic fields by studying the susceptibilities of the measures. The goal of this process is to analytically determine AFM expansion coefficients for a given object shape and potential. Next the numerical accuracy of this method is found using SMSM as a truth model. Lastly, the use of analytical

AFMs is illustrated in a novel electrostatic analysis to investigate the general torque expression of a cylinder-sphere system with a variable center of mass.

Problem Statement

This section establishes the notation and variables used in this paper, as well as the fundamental charging and force models employed and the key binomial expansion used. Consider two charged, conducting neighboring spacecraft as is shown in Fig. 1 with a known charge distribution. This later assumption is relaxed later in the development to assume that only the potentials and relative attitude and separation are known. They each experience a force and torque due to the other's charge. The force and torque on body 2 is found by integrating the differential force, which is a function of body 1's charge distribution, across body 2.

$$\mathrm{d}\boldsymbol{F}_2 = \frac{\mathrm{d}q_1 \mathrm{d}q_2 \boldsymbol{R}}{4\pi\epsilon_0 R^3} \tag{1}$$

where $\boldsymbol{R}$ points from $\mathrm{d}q_1$ to $\mathrm{d}q_2$. The separation vector is expressed from body vectors and a vector between the center of mass of each body $\boldsymbol{R} = \boldsymbol{R}_c + \boldsymbol{r}_2 - \boldsymbol{r}_1$. Using this substitution makes the differential force

$$\mathrm{d}\boldsymbol{F}_2 = \frac{\mathrm{d}q_1 \ \mathrm{d}q_2 \ \boldsymbol{R}_c + \boldsymbol{r}_2 - \boldsymbol{r}_1}{4\pi\epsilon_0 \ ||\boldsymbol{R}_c + \boldsymbol{r}_2 - \boldsymbol{r}_1||^3} \tag{2}$$

where ϵ_0 is the permittivity of free space, $\epsilon_0 \approx 8.854187 * 10^{-12}$ F/m. The differential force is approximated by binomially expanding the denominator and truncating

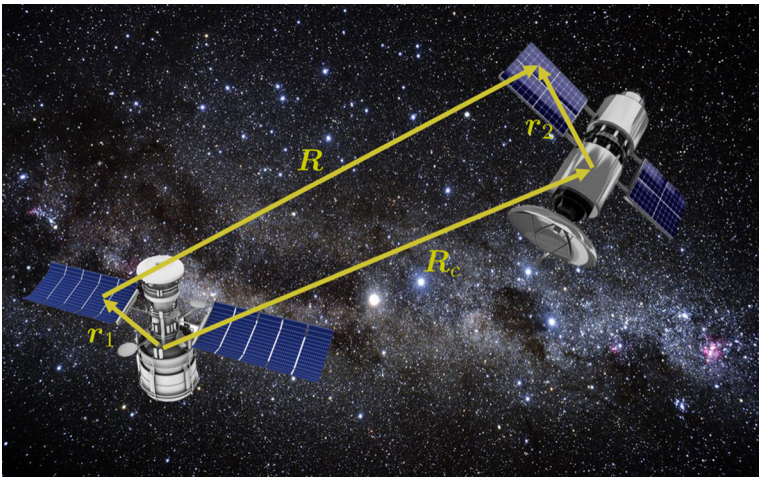

Fig. 1 Coordinate system for inter-craft derivation

higher-order terms on the assumption that the body radii ($\boldsymbol{r}_1$ and $\boldsymbol{r}_2$) are small compared to their separation ($\boldsymbol{R}_c$).

$$\frac{1}{||\boldsymbol{R}_c + \boldsymbol{r}_2 - \boldsymbol{r}_1||^3} = \left(R_c^2 + r_1^2 + r_2^2 + 2\left(\boldsymbol{R}_c \cdot \boldsymbol{r}_2 - \boldsymbol{R}_c \cdot \boldsymbol{r}_1 - \boldsymbol{r}_2 \cdot \boldsymbol{r}_1\right)\right)^{-3/2} \tag{3}$$

$$= \frac{1}{R_c^3}\left[1 + \left(\frac{r_2^2}{R_c^2} + \frac{r_1^2}{R_c^2} + \frac{2}{R_c^2}(\boldsymbol{R}_c \cdot \boldsymbol{r}_2 - \boldsymbol{R}_c \cdot \boldsymbol{r}_1 - \boldsymbol{r}_2 \cdot \boldsymbol{r}_1)\right)\right]^{-3/2} \tag{4}$$

Expand the denominator to second order using a binomial series $(1 + x)^{-3/2} \approx 1 - \frac{3}{2}x + \frac{15}{8}x^2$ and reassemble to approximate the differential force as:

$$\mathrm{d}\boldsymbol{F}_2 = \frac{\mathrm{d}q_1\,\mathrm{d}q_2}{4\pi\epsilon_0 R_c^3}(\boldsymbol{R}_c + \boldsymbol{r}_2 - \boldsymbol{r}_1)\left(1 - \frac{3r_1^2}{2R_c^2} - \frac{3r_2^2}{2R_c^2} - \frac{3(\boldsymbol{R}_c \cdot \boldsymbol{r}_2 - \boldsymbol{R}_c \cdot \boldsymbol{r}_1 - \boldsymbol{r}_2 \cdot \boldsymbol{r}_1)}{R_c^2} + \frac{15((\boldsymbol{R}_c \cdot \boldsymbol{r}_2)^2 + (\boldsymbol{R}_c \cdot \boldsymbol{r}_1)^2 - (\boldsymbol{R}_c \cdot \boldsymbol{r}_1)(\boldsymbol{R}_c \cdot \boldsymbol{r}_2))}{2R_c^4}\right) \tag{5}$$

This differential is integrated over the entire body to obtain the net electrostatic force on this object, or crossed with the body position vector and integrated over the body to obtain torque.

Appropriate Fidelity Measures

Fundamental AFM Expansion Terms Definition

The problem of two charged bodies interacting through electrostatics is similar to two massive bodies interacting through gravity. Just as moments of the mass distribution play a key role in solving the gravitational two-body problem [18], moments of the charge distribution play a key role in predicting electrostatic force and torque. Three especially important moments of the charge distribution are identified and named here:

$$Q = \int_B \mathrm{d}q \qquad \boldsymbol{q} = \int_B \boldsymbol{r}\,\mathrm{d}q \qquad [Q] = \int_B -[\tilde{\boldsymbol{r}}][\tilde{\boldsymbol{r}}]\,\mathrm{d}q \tag{6}$$

Q is a scalar and is the total charge, $\boldsymbol{q}$ is a 3×1 vector and is defined as the dipole moment, and $[Q]$ is a 3×3 tensor defined as the charge tensor. The vector $\boldsymbol{r}$ points from the center of mass to the differential charge $\mathrm{d}q$, and $[\tilde{\boldsymbol{r}}]$ is the matrix form of the vector cross product: $\boldsymbol{a} \times \boldsymbol{b} = [\tilde{\boldsymbol{a}}]\boldsymbol{b}$. If the gravity analogy is used, the total charge Q is similar to the total mass, the dipole moment $\boldsymbol{q}$ is similar to the total mass multiplied by the offset between the center of a coordinate system and the true center of mass, and the charge tensor $[Q]$ is similar to the inertia tensor. The dipole moment $\boldsymbol{q}$ provides a measure of where the center of charge is in relation to the center of mass. If $\boldsymbol{q}$ is zero, then the center of charge and mass locations are identical. To relate these AFM terms to the variables commonly used in multipole expansions, Q and $\boldsymbol{q}$ are the mono and dipole terms, and the charge tensor $[Q]$ defined here is related to the quadrupole $[Q_p]$ by $[Q_p] = -3[Q] + 2\mathrm{tr}([Q])$ [25].

Inter-Craft Electrostatic Reactions

This section derives the force and torque on body 2 due the charge on body 1 and 2. This is done using the 2nd order binomial expansion for the denominator of the differential force.

Force Derivation

The total force on body 2 is found by integrating the differential force over the entire body

$$\boldsymbol{F}_2 = \frac{1}{4\pi\epsilon_0 R_c^3}\int_{B_1}\int_{B_2}(\boldsymbol{R}_c+\boldsymbol{r}_2-\boldsymbol{r}_1)\left(1-\frac{3r_1^2}{2R_c^2}-\frac{3r_2^2}{2R_c^2}-\frac{3(\boldsymbol{R}_c\cdot\boldsymbol{r}_2-\boldsymbol{R}_c\cdot\boldsymbol{r}_1-\boldsymbol{r}_2\cdot\boldsymbol{r}_1)}{R_c^2}+\frac{15((\boldsymbol{R}_c\cdot\boldsymbol{r}_2)^2+(\boldsymbol{R}_c\cdot\boldsymbol{r}_1)^2-(\boldsymbol{R}_c\cdot\boldsymbol{r}_1)(\boldsymbol{R}_c\cdot\boldsymbol{r}_2))}{2R_c^4}\right)\mathrm{d}q_2\mathrm{d}q_1 \tag{7}$$

This equation is broken into three parts: terms resulting from the $\boldsymbol{R}_c, \boldsymbol{r}_1$, and $\boldsymbol{r}_2$ which are denoted as $\boldsymbol{F}_{2_0}$, $\boldsymbol{F}_{2_1}$ and $\boldsymbol{F}_{2_2}$, respectively. The first term $\boldsymbol{F}_{2_0}$ is expressed as

$$\begin{aligned}\boldsymbol{F}_{2_0} &= \frac{\boldsymbol{R}_c}{4\pi\epsilon_0 R_c^3}\int_{B_1}\int_{B_2}\left(1-\frac{3r_1^2}{2R_c^2}-\frac{3r_2^2}{2R_c^2}-\frac{3(\boldsymbol{R}_c\cdot\boldsymbol{r}_2-\boldsymbol{R}_c\cdot\boldsymbol{r}_1-\boldsymbol{r}_2\cdot\boldsymbol{r}_1)}{R_c^2}+\frac{15((\boldsymbol{R}_c\cdot\boldsymbol{r}_2)^2+(\boldsymbol{R}_c\cdot\boldsymbol{r}_1)^2-(\boldsymbol{R}_c\cdot\boldsymbol{r}_1)(\boldsymbol{R}_c\cdot\boldsymbol{r}_2))}{2R_c^4}\right)\mathrm{d}q_2\mathrm{d}q_1\\ &= \frac{\boldsymbol{R}_c}{4\pi\epsilon_0 R_c^3}\left[Q_1Q_2-\left(\frac{3}{2R_c^2}\int_{B_1}r_1^2\,\mathrm{d}q_1\int_{B_2}\mathrm{d}q_2\right)-\left(\frac{3}{2R_c^2}\int_{B_2}r_2^2\,\mathrm{d}q_2\int_{B_1}\mathrm{d}q_1\right)\right.\\ &\quad-\left(\frac{3}{R_c^2}\boldsymbol{R}_c\cdot\int_{B_1}\mathrm{d}q_1\int_{B_2}\boldsymbol{r}_2\mathrm{d}q_2\right)+\left(\frac{3}{R_c^2}\boldsymbol{R}_c\cdot\int_{B_2}\mathrm{d}q_2\int_{B_1}\boldsymbol{r}_1\mathrm{d}q_1\right)\\ &\quad+\left(\frac{3}{R_c^2}\int_{B_1}\boldsymbol{r}_1\mathrm{d}q_2\int_{B_2}\boldsymbol{r}_2\mathrm{d}q_2\right)+\left(\frac{15}{2R_c^4}\int_{B_1}\mathrm{d}q_1\int_{B_2}(\boldsymbol{R}_c\cdot\boldsymbol{r}_2)^2\mathrm{d}q_2\right)\\ &\quad\left.+\left(\frac{15}{2R_c^4}\int_{B_2}\mathrm{d}q_2\int_{B_1}(\boldsymbol{R}_c\cdot\boldsymbol{r}_1)^2\mathrm{d}q_1\right)-\left(\frac{15}{2R_c^4}\int_{B_2}(\boldsymbol{R}_c\cdot\boldsymbol{r}_2)\mathrm{d}q_2\int_{B_1}(\boldsymbol{R}_c\cdot\boldsymbol{r}_1)\mathrm{d}q_1\right)\right]\end{aligned} \tag{8}$$

Here the moments of the charge distribution given in Eq. 6 are used to simplify the equations. Using the identity $\int r^2\mathrm{d}q = \mathrm{tr}([Q])/2$ to simplify the above equation yields:

$$\begin{aligned}\boldsymbol{F}_{2_0} &= \frac{\boldsymbol{R}_c}{4\pi\epsilon_0 R_c^3}\left[Q_1Q_2-\frac{3Q_2}{4R_c^2}\mathrm{tr}([Q_1])-\frac{3Q_1}{4R_c^2}\mathrm{tr}([Q_2])-\frac{3Q_1}{R_c^2}\boldsymbol{R}_c\cdot\boldsymbol{q}_2\right.\\ &\quad+\frac{3Q_2}{R_c^2}\boldsymbol{R}_c\cdot\boldsymbol{q}_1+\frac{3Q_2}{R_c^2}\boldsymbol{q}_2\cdot\boldsymbol{q}_1+\frac{15Q_1}{2R_c^4}\int_{B_2}(\boldsymbol{R}_c\cdot\boldsymbol{r}_2)^2\mathrm{d}q_2\\ &\quad\left.+\frac{15Q_2}{2R_c^4}\int_{B_1}(\boldsymbol{R}_c\cdot\boldsymbol{r}_1)^2\mathrm{d}q_1-\frac{15}{2R_c^4}(\boldsymbol{R}_c\cdot\boldsymbol{q}_2)(\boldsymbol{R}_c\cdot\boldsymbol{q}_1)\right)\right]\end{aligned} \tag{9}$$

To solve the two remaining integrals, apply the vector identity $(\boldsymbol{a}\cdot\boldsymbol{b})\boldsymbol{b} = ([\tilde{\boldsymbol{b}}][\tilde{\boldsymbol{b}}]+ b^2[I])\boldsymbol{a}$ to the terms of the form $(\boldsymbol{R}_c\cdot\boldsymbol{r})^2$ and integrate to yield

$$\boldsymbol{R}_c\cdot(\boldsymbol{R}_c\cdot\boldsymbol{r})\boldsymbol{r} = \boldsymbol{R}_c\cdot([\tilde{\boldsymbol{r}}][\tilde{\boldsymbol{r}}]+r^2[I])\boldsymbol{R}_c = \boldsymbol{R}_c^T[\tilde{\boldsymbol{r}}][\tilde{\boldsymbol{r}}]\boldsymbol{R}_c + R_c^2r^2 \tag{10}$$

$$\rightarrow -\boldsymbol{R}_c^T[Q]\boldsymbol{R}_c + R_c^2\mathrm{tr}([Q])/2 \tag{11}$$

and re-write $\boldsymbol{F}_{2_0}$ finally as:

$$\boldsymbol{F}_{2_0} = \frac{\boldsymbol{R}_c}{4\pi\epsilon_0 R_c^3}\left[Q_1Q_2 + \frac{3Q_2}{R_c^2}\mathrm{tr}([Q_1]) + \frac{3Q_1}{R_c^2}\mathrm{tr}([Q_2]) - \frac{3Q_1}{R_c^2}\boldsymbol{R}_c\cdot\boldsymbol{q}_2 + \frac{3Q_2}{R_c^2}\boldsymbol{R}_c\cdot\boldsymbol{q}_1 + \frac{3Q_2}{R_c^2}\boldsymbol{q}_2\cdot\boldsymbol{q}_1 - \frac{15Q_1}{2R_c^4}\boldsymbol{R}_c^T[Q_2]\boldsymbol{R}_c - \frac{15Q_2}{2R_c^4}\boldsymbol{R}_c^T[Q_1]\boldsymbol{R}_c - \frac{15}{R_c^4}(\boldsymbol{R}_c\cdot\boldsymbol{q}_2)(\boldsymbol{R}_c\cdot\boldsymbol{q}_1)\right] \tag{12}$$

The second part of the force $\boldsymbol{F}_{2_1}$ is much simpler because many of the terms become third order and are neglected in this second order expansion.

$$\boldsymbol{F}_{2_1} = \frac{1}{4\pi\epsilon_0 R_c^3}\int_{B_1}\int_{B_2}\boldsymbol{r}_2\left(1-\frac{3(\boldsymbol{R}_c\cdot\boldsymbol{r}_2-\boldsymbol{R}_c\cdot\boldsymbol{r}_1)}{R_c^2}\right)\mathrm{d}q_2\mathrm{d}q_1 \tag{13}$$

$$= \frac{1}{4\pi\epsilon_0 R_c^3}\left[Q_1\boldsymbol{q}_2 + \frac{3Q_1}{R_c^2}[Q_2]\boldsymbol{R}_c - \frac{3Q_1}{2R_c^2}\mathrm{tr}([Q_2])\boldsymbol{R}_c + \frac{3(\boldsymbol{R}_c\cdot\boldsymbol{q}_1)}{R_c^2}\boldsymbol{q}_2\right] \tag{14}$$

The third part of the force $\boldsymbol{F}_{2_2}$ is similar in form to $\boldsymbol{F}_{2_1}$ with the $\boldsymbol{r}_2$ being replaced with a $-\boldsymbol{r}_1$.

$$\boldsymbol{F}_{2_2} = \frac{1}{4\pi\epsilon_0 R_c^3}\int_{B_1}\int_{B_2}-\boldsymbol{r}_1\left(1-\frac{3(\boldsymbol{R}_c\cdot\boldsymbol{r}_2-\boldsymbol{R}_c\cdot\boldsymbol{r}_1)}{R_c^2}\right)\mathrm{d}q_2\mathrm{d}q_1 \tag{15}$$

$$= \frac{1}{4\pi\epsilon_0 R_c^3}\left[-Q_2\boldsymbol{q}_1 + \frac{3Q_2}{R_c^2}[Q_1]\boldsymbol{R}_c - \frac{3Q_2}{2R_c^2}\mathrm{tr}([Q_1])\boldsymbol{R}_c + \frac{3(\boldsymbol{R}_c\cdot\boldsymbol{q}_2)}{R_c^2}\boldsymbol{q}_1\right] \tag{16}$$

The total force is then expressed as

$$\boldsymbol{F}_2 = \frac{1}{4\pi\epsilon_0 R_c^3}\left[\left(Q_1Q_2 + \frac{3Q_2}{2R_c^2}\mathrm{tr}([Q_1]) + \frac{3Q_1}{2R_c^2}\mathrm{tr}([Q_2]) - \frac{3Q_1}{R_c^2}\boldsymbol{R}_c\cdot\boldsymbol{q}_2 + \frac{3Q_2}{R_c^2}\boldsymbol{R}_c\cdot\boldsymbol{q}_1 + \frac{3Q_2}{R_c^2}\boldsymbol{q}_2\cdot\boldsymbol{q}_1 - \frac{15Q_1}{2R_c^4}\boldsymbol{R}_c^T[Q_2]\boldsymbol{R}_c - \frac{15Q_2}{2R_c^4}\boldsymbol{R}_c^T[Q_1]\boldsymbol{R}_c - \frac{15}{R_c^4}(\boldsymbol{R}_c\cdot\boldsymbol{q}_2)(\boldsymbol{R}_c\cdot\boldsymbol{q}_1)\right)\boldsymbol{R}_c + Q_1\boldsymbol{q}_2 + \frac{3Q_1}{R_c^2}[Q_2]\boldsymbol{R}_c + \frac{3(\boldsymbol{R}_c\cdot\boldsymbol{q}_1)}{R_c^2}\boldsymbol{q}_2 - Q_2\boldsymbol{q}_1 + \frac{3Q_2}{R_c^2}[Q_1]\boldsymbol{R}_c + \frac{3(\boldsymbol{R}_c\cdot\boldsymbol{q}_2)}{R_c^2}\boldsymbol{q}_1\right] \tag{17}$$

This equation is visualized in Table 1, where the common factor of $4\pi\epsilon_0 R_c^3$ is omitted, allowing easy ordering of terms based on which measures $(Q, \boldsymbol{q}, [Q])$ they incorporate. They are also ordered by the dimensionless ratio r/R_c where r is a characteristic dimension of either spacecraft. As the spacecraft move farther and farther away, the higher order terms in this variable matter less and less. The zeroth order term is in the upper left, the two boxes with two terms each are the first order terms, and the three boxes containing twelve terms along the diagonal are the second order terms. This table allows easy selection of the force terms needed for appropriate fidelity.

Table 1 Force ordering matrix

	Q_1	$\boldsymbol{q}_1$	$[Q_1]$
Q_2	$Q_1 Q_2 \boldsymbol{R}_c$	$\frac{3Q_2}{R_c^2}(\boldsymbol{R}_c \cdot \boldsymbol{q}_1)\boldsymbol{R}_c - Q_2 \boldsymbol{q}_1$	$\frac{3Q_2}{2R_c^2}\mathrm{tr}([Q_1])\boldsymbol{R}_c$ $-\frac{15Q_2}{2R_c^4}(\boldsymbol{R}_c^T[Q_1]\boldsymbol{R}_c)\boldsymbol{R}_c$ $+\frac{3Q_2}{R_c^2}[Q_1]\boldsymbol{R}_c$
$\boldsymbol{q}_2$	$Q_1 \boldsymbol{q}_2 - \frac{3Q_1}{R_c^2}(\boldsymbol{R}_c \cdot \boldsymbol{q}_2)\boldsymbol{R}_c$	$\frac{3}{R_c^2}(\boldsymbol{q}_2 \cdot \boldsymbol{q}_1)\boldsymbol{R}_c$ $-\frac{15}{R_c^4}(\boldsymbol{R}_c \cdot \boldsymbol{q}_2)(\boldsymbol{R}_c \cdot \boldsymbol{q}_1)\boldsymbol{R}_c$ $+\frac{3(\boldsymbol{R}_c \cdot \boldsymbol{q}_1)}{R_c^2}\boldsymbol{q}_2 + \frac{3(\boldsymbol{R}_c \cdot \boldsymbol{q}_2)}{R_c^2}\boldsymbol{q}_1$	
$[Q_2]$	$\frac{3Q_1}{2R_c^2}\mathrm{tr}([Q_2])\boldsymbol{R}_c$ $-\frac{15Q_1}{2R_c^4}(\boldsymbol{R}_c^T[Q_2]\boldsymbol{R}_c)\boldsymbol{R}_c$ $+\frac{3Q_1}{R_c^2}[Q_2]\boldsymbol{R}_c$		

As might be expected, the force expression is symmetric, if one changes the sign on all $\boldsymbol{R}_c$ terms and switches the subscripts the force on body 1 is found to be equal in magnitude but opposite in direction to the force on body 2. This satisfies Newton's 3rd law.

Torque Derivation

The torque on body 2 is given by $\boldsymbol{T}_2 = \int_{B_1}\int_{B_2} \boldsymbol{r}_2 \times \mathrm{d}\boldsymbol{F}$, where the same binomial expansion as before is used to approximate $\mathrm{d}\boldsymbol{F}$ to second order.

$$\boldsymbol{T}_2 = \frac{1}{4\pi\epsilon_0 R_c^3}\int_{B_1}\int_{B_2} \boldsymbol{r}_2 \times (\boldsymbol{R}_c + \boldsymbol{r}_2 - \boldsymbol{r}_1)\left(1 - \frac{3(\boldsymbol{R}_c \cdot \boldsymbol{r}_2 - \boldsymbol{R}_c \cdot \boldsymbol{r}_1)}{R_c^2}\right)\mathrm{d}q_2\mathrm{d}q_1 \tag{18}$$

Because of the extra $\boldsymbol{r}_2$, many of the terms in the differential force expansion become third order and are neglected. The differential torque has three parts corresponding to the $\boldsymbol{r}_2 \times \boldsymbol{R}_c$, $\boldsymbol{r}_2 \times \boldsymbol{r}_2$ and $\boldsymbol{r}_2 \times \boldsymbol{r}_1$ components. The middle term is zero and the first and third are labeled by $\boldsymbol{T}_{2_0}$ and $\boldsymbol{T}_{2_1}$, respectively. $\boldsymbol{T}_{2_0}$ is evaluated first:

$$\boldsymbol{T}_{2_0} = \frac{1}{4\pi\epsilon_0 R_c^3}\int_{B_1}\int_{B_2} \boldsymbol{r}_2 \times \boldsymbol{R}_c\left(1 - \frac{3(\boldsymbol{R}_c \cdot \boldsymbol{r}_2 - \boldsymbol{R}_c \cdot \boldsymbol{r}_1)}{R_c^2}\right)\mathrm{d}q_2\mathrm{d}q_1 \tag{19}$$

$$= -\frac{1}{4\pi\epsilon_0 R_c^3}\boldsymbol{R}_c \times \int_{B_1}\int_{B_2} \boldsymbol{r}_2\left(1 - \frac{3(\boldsymbol{R}_c \cdot \boldsymbol{r}_2 - \boldsymbol{R}_c \cdot \boldsymbol{r}_1)}{R_c^2}\right)\mathrm{d}q_2\mathrm{d}q_1 \tag{20}$$

where higher order terms in the binomial expansion are neglected. The integral is identical to the force integral in Eq. 13 evaluated earlier, and is written down from inspection as:

$$\boldsymbol{T}_{2_0} = -\frac{1}{4\pi\epsilon_0 R_c^3}\boldsymbol{R}_c \times \left[\frac{Q_1\boldsymbol{q}_2}{R_c^3} + \frac{3(\boldsymbol{R}_c \cdot \boldsymbol{q}_1)\boldsymbol{q}_2}{R_c^5} + \frac{3Q_1[Q_2]\boldsymbol{R}_c}{R_c^5}\right] \tag{21}$$

The other part of the torque comes from the $\boldsymbol{r}_1$ and is evaluated below:

$$\boldsymbol{T}_{2_1} = -\frac{1}{4\pi\epsilon_0 R_c^3}\int_{B_1}\int_{B_2}(\boldsymbol{r}_2 \times \boldsymbol{r}_1)\mathrm{d}q_2\mathrm{d}q_1 \tag{22}$$

The binomial expansion here is truncated to just the first term because the $\boldsymbol{r}_2 \times \boldsymbol{r}_1$ term is already second order. This gives

$$\boldsymbol{T}_{2_1} = -\frac{1}{4\pi\epsilon_0 R_c^3}\boldsymbol{q}_2 \times \boldsymbol{q}_1 \tag{23}$$

The total torque is found by summing $\boldsymbol{T}_{2_0}$ and $\boldsymbol{T}_{2_1}$ to yield

$$\boldsymbol{T}_2 = \frac{1}{4\pi\epsilon_0 R_c^3}\left[Q_1\boldsymbol{q}_2 \times \boldsymbol{R}_c + \frac{3(\boldsymbol{R}_c \cdot \boldsymbol{q}_1)\boldsymbol{q}_2 \times \boldsymbol{R}_c}{R_c^2} - \frac{3Q_1\boldsymbol{R}_c \times [Q_2]\boldsymbol{R}_c}{R_c^2} + (\boldsymbol{q}_1 \times \boldsymbol{q}_2)\right] \tag{24}$$

This equation is visualized in Table 2 which follows Table 1 in omitting the factor of $4\pi\epsilon_0 R_c^3$ and grouping terms by their order in the dimensionless ratio r/R_c. Terms closer to the upper left corner are lower order.

As expected, there are no zeroth order terms, in fact there are no terms at all corresponding to the scalar charge Q_2. Unlike the force expansion in which the forces are equal and opposite, the torque is not symmetric, i.e. $\boldsymbol{T}_1 \neq -\boldsymbol{T}_2$. This is because the torque on body 1 and body 2 are not measured about the same point, but rather the center of mass of each body. If all torques are measured about the same point, such as the barycenter of the system, the torques are equal and opposite since the forces are equal and opposite. Thus, they cancel out and are not able to change the angular momentum of the system.

Radial Electrostatic Field Simplification

In Reference [19], the force and torque on a charged body in a radial field are found by assuming a differential force of

$$\mathrm{d}\boldsymbol{F}_2 = \frac{Q_1\mathrm{d}q_2}{4\pi\epsilon_0 R^3}\boldsymbol{R} \tag{25}$$

and integrating over body 2. Rather than repeating this integration, the force and torque can be produced by summing the terms in the first column of the force and torque tables (Tables 1 and 2) which only consider the scalar charge of body 1. This

Table 2 Torque ordering matrix

	Q_1	$\boldsymbol{q}_1$	$[Q_1]$
Q_2			
$\boldsymbol{q}_2$	$Q_1\boldsymbol{q}_2 \times \boldsymbol{R}_c$	$\frac{3}{R_c^2}(\boldsymbol{R}_c \cdot \boldsymbol{q}_1)\boldsymbol{q}_2 \times \boldsymbol{R}_c + (\boldsymbol{q}_1 \times \boldsymbol{q}_2)$	
$[Q_2]$	$-\frac{3}{R_c^2}Q_1\boldsymbol{R}_c \times [Q_2]\boldsymbol{R}_c$		

works because if body 1 has only a scalar charge, it is a point charge and creates a purely radial field. This yields

$$\boldsymbol{F}_2 = \frac{Q_1}{4\pi\epsilon_0 R_c^3}\left[Q_2\boldsymbol{R}_c + \boldsymbol{q}_2 - \frac{3(\boldsymbol{q}\cdot\boldsymbol{R}_c)}{R_c^2}\boldsymbol{R}_c + \frac{3[Q_2]\boldsymbol{R}_c}{R_c^2} + \frac{3\boldsymbol{R}_c}{2R_c^2}\mathrm{tr}([Q_2]) - \frac{15}{2R_c^4}(\boldsymbol{R}_c^T[Q_2]\boldsymbol{R}_c)\boldsymbol{R}_c\right] \tag{26}$$

$$\boldsymbol{L}_2 = \frac{Q_1}{4\pi\epsilon_0 R_c^3}\left[\boldsymbol{q}_2 + \frac{3}{R_c^2}[Q_2]\boldsymbol{R}_c\right]\times\boldsymbol{R}_c \tag{27}$$

which agrees with the derivation done with the point charge differential force. This shows how force and torque in a radial field is a special case of the general two body problem. This is similar to how in most treatments a satellite is treated as a point mass while the earth is treated as a general body using spherical harmonics.

Flat Electrostatic Field Simplification

It is also of interest to calculate the force and torque on charged conducting bodies due to ambient flat electric and magnetic fields [20]. The differential force on a differential charge moving at $\boldsymbol{v}$ subject to $\boldsymbol{E}$ and $\boldsymbol{B}$ fields is given in Reference [14] as:

$$\mathrm{d}\boldsymbol{F} = \mathrm{d}q(\boldsymbol{E} + \boldsymbol{v}\times\boldsymbol{B}) \tag{28}$$

This differential force only varies significantly across a body if it is rotating very quickly near the geostationary point. The velocity is the orbital velocity $\boldsymbol{v}_o$ plus the transport velocity: $\boldsymbol{\omega}_{\mathcal{B}/\mathcal{E}}\times\boldsymbol{r}$ [32], where $\boldsymbol{\omega}_{\mathcal{B}/\mathcal{E}}$ is the angular velocity between the satellite body frame $\mathcal{B}$ and the magnetic field frame $\mathcal{E}$. For a spacecraft with $r = 1$ m, $\omega_{\mathcal{B}/\mathcal{E}} = 1$ deg/sec, and an ECEF orbital velocity of 1 km/sec, the ratio of the transport velocity to the orbital velocity will be less than 10^{-5}. In many scenarios the transport term can be dropped. The force is then:

$$\boldsymbol{F} = \int_B (\boldsymbol{E} + \boldsymbol{v}_o\times\boldsymbol{B})\mathrm{d}q = Q(\boldsymbol{E} + \boldsymbol{v}_o\times\boldsymbol{B}) \tag{29}$$

and the torque is

$$\boldsymbol{L} = \int_B \boldsymbol{r}\times(\boldsymbol{E} + \boldsymbol{v}_o\times\boldsymbol{B})\mathrm{d}q = -(\boldsymbol{E} + \boldsymbol{v}_o\times\boldsymbol{B})\times\boldsymbol{q} \tag{30}$$

This is the exact answer for the torque on a pure dipole in a flat field [11, 14].

Susceptibilities of the Measures

The expansions for force and torque in the electrostatic two-body problem, radial field, and flat field are useful formula. However, they rely on knowledge of the charge distribution on both bodies in order to perform the integrations and find the measures. Unlike the gravitational two-body problem, these measures change as charge moves throughout the bodies. Recalculating the entire charge distribution for both bodies would be a very intensive process. Here, a method for predicting the measures

from parameters that are much more feasible to measure in situ such as the voltage, attitude, and position of each craft is presented.

To do this, a matrix dependent on the relative position and attitude is used to translate the voltage of each craft into a representation of the charge distribution. From this distribution, the measures are formed as functions of the voltage of each craft. There are many ways to make this matrix, including the Method of Moments or Boundary Element Method. A recent addition is the Multi-Sphere Method, which uses hand-tuned parameters for the size and locations of spheres which are constrained to be equipotential [36, 37].

MSM emerged as a way to predict the force and torque with high-enough fidelity to be useful, while also evaluating fast enough to be practical. MSM approximates the satellite as a collection of spheres with variable position and radii. The voltage of any sphere is a function of both its own charge and the charge on neighboring spheres. If these spheres are far enough away to be approximated as point charges, the voltage on the i^{th} sphere is given by: [14, 36, 37]

$$V_i = \frac{1}{4\pi\epsilon_0}\frac{q_i}{R_i} + \sum_{j=1,\, j\neq i}^{N} \frac{1}{4\pi\epsilon_0}\frac{q_j}{r_{i,\,j}} \tag{31}$$

where q_i and R_i are the charge and radius of the i^{th} sphere, respectively, and $r_{i,\,j}$ is the distance between spheres i and j. If the voltages of each sphere are given by $\boldsymbol{V} = [V_1, V_2, \ldots V_N]^T$ and the charges are given by $\boldsymbol{Q} = [q_1, q_2, \ldots q_N]^T$, the relationship between the two is $\boldsymbol{V} = [S]\boldsymbol{Q}$ or $\boldsymbol{Q} = [C]\boldsymbol{V}$, where $[C]$ is the capacitance matrix and $[S]$ is the elastance matrix defined below [35]:

$$[S] = \frac{1}{4\pi\epsilon_0}\begin{bmatrix} 1/R_1 & 1/r_{1,2} & \cdots & 1/r_{1,N} \\ 1/r_{2,1} & 1/R_2 & \cdots & r_{2,N} \\ \vdots & \vdots & \ddots & \vdots \\ 1/r_{N,1} & 1/r_{N,2} & \cdots & 1/R_N \end{bmatrix} \tag{32}$$

Since the voltage is assumed known, the charge distribution is found by numerically solving the linear system. If two conductors with n_1 and n_2 spheres each are considered, the elastance matrix can be put into block form:

$$\begin{bmatrix} \boldsymbol{V}_1 \\ \boldsymbol{V}_2 \end{bmatrix} = \frac{1}{4\pi\epsilon_0}\begin{bmatrix} S_1 & S_M \\ S_M^T & S_2 \end{bmatrix}\begin{bmatrix} \boldsymbol{Q}_1 \\ \boldsymbol{Q}_2 \end{bmatrix} \tag{33}$$

where the voltage and charge of each craft are separated. Note that the self elastance terms S_1 and S_2 are much larger than the mutual elastance terms S_M because the inter-sphere separations are much smaller inside one body rather than between the two bodies. Additionally, the self elastance matrices contain the diagonal $1/R$ terms which are larger than the off-diagonal $1/r$ terms. As an example, consider a template box and panel spacecraft with an 8 m boom made from 248 spheres and a 3×1 m cylinder made from 138 spheres. The log of the elastance matrix for these two objects with a separation of 40 m is shown in Fig. 2. This figure uses color to show the size of elements of the matrix; each element of the matrix is converted to a colored square at an x, y position corresponding to the row and column.

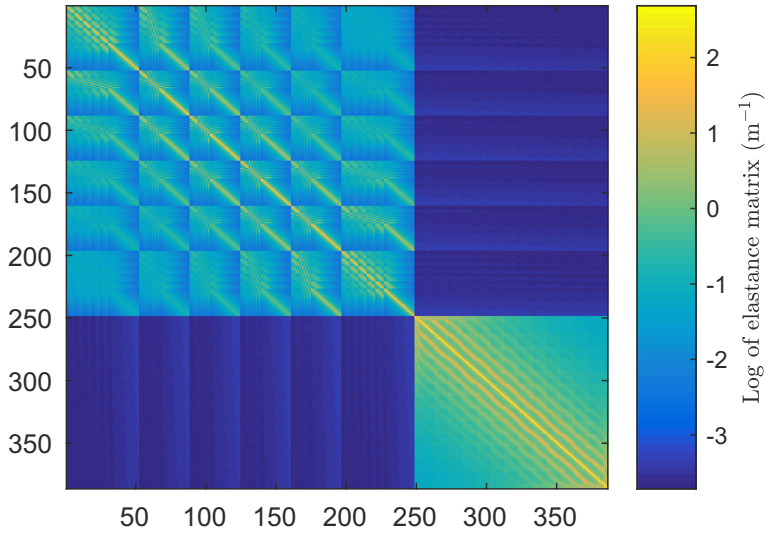

Fig. 2 Log of elastance matrix. X and y axes are row and column numbers

There are clearly four blocks, and the diagonals are $10^2 - 10^5$ times larger than the non-diagonal blocks. The blocky structure in the upper diagonal block comes from the method of assembly for the the box and panel spacecraft which is made from six rectangles. In general, the diagonal blocks will not change with relative position or attitude. The blocky structure, symmetry, and the time-fixed properties of the diagonal blocks are exploited when inverting using the Schur complement.

$$\begin{bmatrix} A & B \\ B^T & D \end{bmatrix}^{-1} = \begin{bmatrix} (A - BD^{-1}B^T)^{-1} & -A^{-1}B(D - B^TA^{-1}B)^{-1} \\ -D^{-1}B^T(A - BD^{-1}B^T)^{-1} & (D - B^TA^{-1}B)^{-1} \end{bmatrix} \tag{34}$$

Recognizing that A and D represent the self capacitance matrices, which contain much larger terms than the mutual matrix B, terms second order in B are dropped:

$$\begin{bmatrix} A & B \\ B^T & D \end{bmatrix}^{-1} \approx \begin{bmatrix} A^{-1} & -A^{-1}BD^{-1} \\ -D^{-1}B^TA^{-1} & D^{-1} \end{bmatrix} = \begin{bmatrix} C_1 & -C_1S_MC_2 \\ -C_2S_M^TC_1 & C_2 \end{bmatrix} \tag{35}$$

where $[C_i] = [S_i]^{-1}$ for all blocks. The two matrices C_1 and C_2 are not functions of the relative separation and orientation, which means they will be constant in time. The terms in S_M are of the form $1/||\boldsymbol{R}_c + \boldsymbol{r}_{2_i} - \boldsymbol{r}_{1_j}||$. Since the center to center separation R_c is much greater than the dimensions of either craft r_1 or r_2, this is approximated as

$$[S_M]_{i,j} = \frac{1}{||\boldsymbol{R}_c + \boldsymbol{r}_{2_i} - \boldsymbol{r}_{1_j}||} \sim \frac{1}{R_c} \tag{36}$$

Approximating all elements in the mutual capacitance matrix as $1/R_c$ assumes that all spheres are located at the center of mass of the other craft for the purposes of inverting the elastance matrix. This loses the dependence on relative attitude but cap-

tures the first order mutual capacitance and susceptibility. The elastance matrix is now approximately inverted as

$$\begin{bmatrix} \boldsymbol{Q}_1 \\ \boldsymbol{Q}_2 \end{bmatrix} = \frac{1}{4\pi\epsilon_0} \begin{bmatrix} C_1 & -C_1\mathbb{1}(n_1,n_2)C_2/R_c \\ -C_2\mathbb{1}(n_2,n_1)C_1/R_c & C_2 \end{bmatrix} \begin{bmatrix} \boldsymbol{V}_1 \\ \boldsymbol{V}_2 \end{bmatrix} \tag{37}$$

where $\mathbb{1}(n,m)$ is a matrix consisting of ones of size (n,m). If the two bodies are both conductors, each MSM sphere is at the same voltage and this matrix equation is transformed to a vector equation

$$\boldsymbol{Q}_1 = [C_1]\mathbb{1}(n_1,1)V_1 - \frac{[C_1]\mathbb{1}(n_1,n_2)[C_2]}{R_c}\mathbb{1}(n_2,1)V_2 \tag{38}$$

$$\boldsymbol{Q}_2 = [C_2]\mathbb{1}(n_2,1)V_2 - \frac{[C_2]\mathbb{1}(n_2,n_1)[C_1]}{R_c}\mathbb{1}(n_1,1)V_1 \tag{39}$$

Now the charge on each MSM sphere is approximated as a function of a collection of matrices that do not change with state, and the scalar voltage of each craft. The susceptibility of the total charges, dipoles, and charge tensors to the voltage of each craft are found next.

Total Charges

The total charge on each spacecraft is found by summing the charge on each sphere

$$Q = \sum_{i=1}^{n_1} q_i = \mathbb{1}(1,n)\,\boldsymbol{Q} \tag{40}$$

Thus, the scalar charge of body 1 is given by

$$Q_1 = C_S V_1 + C_M V_2 \tag{41}$$

where the self and mutual capacitances are given by

$$C_S = \mathbb{1}(1,n_1)[C_1]\mathbb{1}(n_1,1) = \sum_{i=1}^{n_1}\sum_{j=1}^{n_1}[C_1]_{i,j} \tag{42}$$

$$C_M = \frac{-\mathbb{1}(1,n_2)[C_1]\mathbb{1}(n_1,n_2)[C_2]\mathbb{1}(n_2,1)}{R_c} = -\frac{\sum_{i=1}^{n_1}\sum_{j=1}^{n_2}[C_1]\mathbb{1}(n_1,n_2)[C_2]}{R_c} \tag{43}$$

The scalar self capacitance can be computed with high fidelity using a MSM model with hundreds or thousands of spheres and re-used in each time step for computation. The numerator of the mutual capacitance can be similarly computed at high fidelity and then divided by the norm of the separation vector at each time step.

Dipole Moments

The dipole $\boldsymbol{q}$ is defined in a continuous charge distribution and MSM model as

$$\boldsymbol{q} = \int_B \boldsymbol{r}\,\mathrm{d}q = \sum_{i=1}^{N} \boldsymbol{r}_i q_i = [R]\boldsymbol{q} \tag{44}$$

where $[R]$ is a $3 \times N$ matrix containing the x, y, and z coordinates of each MSM sphere:

$$[R] = \begin{bmatrix} x_1 & \dots & x_N \\ y_1 & \dots & y_N \\ z_1 & \dots & z_N \end{bmatrix} \tag{45}$$

The dipole is given by

$$\boldsymbol{q} = \boldsymbol{\chi}_S V_1 + \boldsymbol{\chi}_M V_2 \tag{46}$$

where the self and mutual susceptibilities of the dipole for body 1 are

$$\boldsymbol{\chi}_S = [R_1][C_1]\mathbb{1}(n_1, 1) \tag{47}$$

$$\boldsymbol{\chi}_M = \frac{-[R_1][C_1]\mathbb{1}(n_1, n_2)[C_2]\mathbb{1}(n_2, 1)}{R_c} \tag{48}$$

Once again, these 3×1 vectors can be computed with high fidelity from SMSM models of each body. Each element in the mutual term must be divided by the separation distance, which may change with time.

Charge Tensor

The charge tensor is defined from a continuous charge distribution or MSM model as

$$[Q] = \int_B -[\tilde{\boldsymbol{r}}][\tilde{\boldsymbol{r}}]\mathrm{d}q = \sum_i^N - [\tilde{\boldsymbol{r}_i}][\tilde{\boldsymbol{r}_i}]q_i \tag{49}$$

Define $[R_s]$ as a $3 \times 3N$ matrix containing the cross product matrix of each MSM sphere position and B is a $3N \times N$ matrix used to interweave three copies of the charge vector made from smaller matrices b.

$$[R_s] = \begin{bmatrix} [\tilde{\boldsymbol{r}_l}] \\ \vdots \\ [\tilde{\boldsymbol{r}_N}] \end{bmatrix} \qquad [b] = \begin{bmatrix} 1 \\ 1 \\ 1 \end{bmatrix} \qquad [B] = \begin{bmatrix} b & 0 & \dots & 0 \\ 0 & b & \dots & 0 \\ \vdots & \vdots & \ddots & \vdots \\ 0 & 0 & \dots & b \end{bmatrix} \tag{50}$$

The charge tensor is now found as a function of both voltages, and two 3×3 matrices,

$$[Q_1] = [\psi_S]V_1 + [\psi_M]V_2 \tag{51}$$

where the self and mutual susceptibilities of the charge tensor for body 1 are given by

$$[\psi_S] = [R_{s_1}]^T \mathrm{diag}([B][C_1]\mathbb{1}(n_1, 1))[R_{s_1}] \tag{52}$$

$$[\psi_M] = -[R_{s_1}]^T \frac{\mathrm{diag}([B][C_1]\mathbb{1}(n_1, n_2)[C_2]\mathbb{1}(n_2, 1))}{R_c}[R_{s_1}] \tag{53}$$

These matrices can be found using high fidelity MSM models before propagation and the mutual term can be adjusted by dividing by the separation distance. The derivations are done for body 1, but the susceptibilities for body 2 can easily be found by changing all subscript 2s to 1s and vice versa.

Flat Field Susceptibilities

A flat environmental field will change the charge distribution, but not the scalar charge. The only measures that contribute in a flat field are the dipole and the total charge. The scalar charge is still given by

$$Q = CV \tag{54}$$

To find the dipole, write the voltage of each sphere as a function both of the charges and its position relative to the total field $\boldsymbol{A} = \boldsymbol{E} + \boldsymbol{v} \times \boldsymbol{B}$ where $\boldsymbol{v}$ is the velocity with respect to the magnetic field.

$$\boldsymbol{V} = [C]^{-1}\boldsymbol{Q} - [R]^T\boldsymbol{A} \tag{55}$$

The charges are found by

$$\boldsymbol{Q} = [C](\boldsymbol{V} - [R]^T\boldsymbol{A}) \tag{56}$$

The dipole is then

$$\boldsymbol{q} = \boldsymbol{\chi}_S V_T + [\chi_A]\boldsymbol{A} \tag{57}$$

where the self and ambient susceptibilities are given by

$$\boldsymbol{\chi}_S = [R][C]\mathbb{1}(n, 1) \tag{58}$$

$$[\chi_A] = [R][C][R]^T \tag{59}$$

for a model with n spheres. The ambient susceptibility is similar to the electric susceptibility used to calculate the polarization of dielectrics in an electric field [14].

Numerical Validation

In a flat field, AFMs and MSM give the same answers down to machine precision assuming the same MSM model is used to calculate the susceptibilities of the measures because there is no truncation of a binomial series. For the two-body problem, the accuracy of predictive AFMs is checked against the truth model of SMSM, which places a large number of equal radius spheres uniformly across the surface of the body. The radius of all spheres is varied to achieve the known self capacitance. Although this method is slower to evaluate (due to the much larger number of spheres), it removes the need for hand tuning and has good accuracy relative to commercial FEA software [38]. An example SMSM model for two template "box and panel" spacecraft in close proximity is shown in Fig. 3. Note that charge, which is shown as color, tends to bunch up at the corners of conductors and is affected by the nearby spacecraft.

For validation, one "box and panel" spacecraft has fixed location and attitude at the origin of the coordinate system. The second spacecraft occupies many different positions and attitudes on a shell of a given radius. SMSM is used to find the force and torque on the fixed craft. The force and torque is also predicted using AFMs with the susceptibilities $C_S, C_M, \boldsymbol{\chi}_S, \boldsymbol{\chi}_M, [\psi_S]$, and $[\psi_M]$ for each craft found before

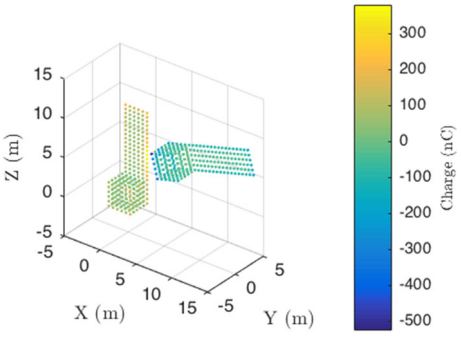

Fig. 3 Example SMSM configuration for two satellites

computation from the same 256-sphere SMSM model. The average percent error is computed for each spherical shell. The percentage error is computed as:

$$PE = 100 * \frac{||\boldsymbol{a}_{\mathrm{AFM}} - \boldsymbol{a}_{\mathrm{T}}||}{||\boldsymbol{a}_{\mathrm{T}}||} \tag{60}$$

where $\boldsymbol{a}$ is either the force or torque, and the subscript "T" indicates the truth model.

The second craft is placed at points on a spherical shell precomputed using a golden spiral algorithm [1] which arranges 20 points equidistantly on the surface of a sphere. The shells are varied in radius logarithmically from 15 to 200 m in 10 steps. The attitude of the second object at each of these points is changed using three random Euler angles while the first object is held fixed in attitude at the origin. The mean percentage error per shell is shown in Fig. 4.

The mean percentage error for the zeroth, first, and second order expressions for force are shown as red, green, and blue lines in the force plot. Since there is no zeroth order term for torque prediction, only the first and second order expressions are shown in the torque plot. A dashed line is shown 1 standard deviation above each of these to give a sense of the variation a user should expect.

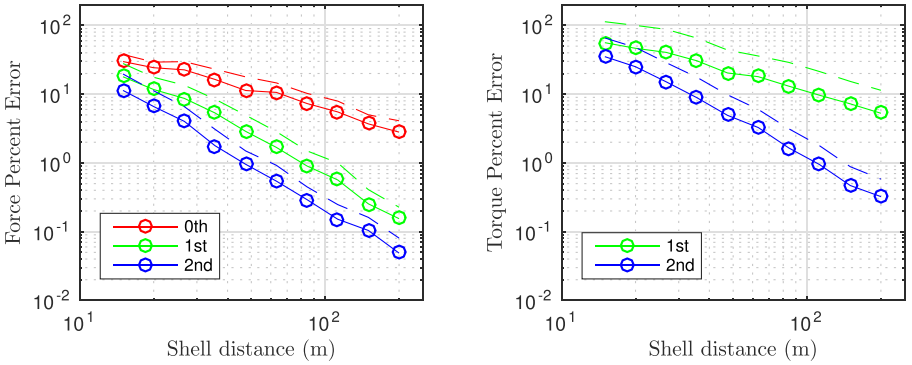

(a) Force percent error (b) Torque percent error

Fig. 4 Percentage errors for force and torque using predictive AFMs

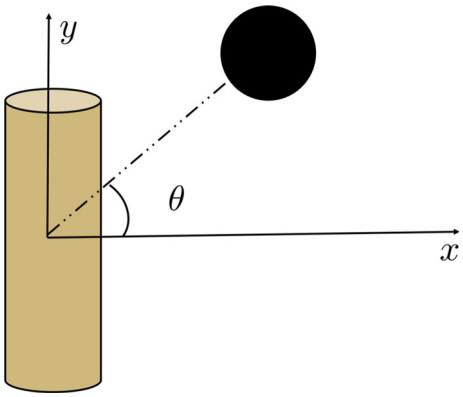

Fig. 5 Coordinate system for example analysis

The errors are initially very high, a few tens of percent on average depending on order, but they drop quickly as the spacecraft move farther apart. Since the AFM derivation hinges on the assumption that the spacecraft sizes are much smaller than the distance between them, this matches intuition. The second order term for force drops below 5% error at 25 m and the second order term for torque drops below 5% at 48 m.

Analysis and Applications

There are many numerical methods for electrostatic force and torque prediction for conductors. However, they do not give good analytical forms for force and torque. This section summarizes previous work that curve fit the angular and voltage dependencies of electrostatic torque, and then uses AFMs to analytically predict the same result. Next AFMs are used to predict the torque in the case where the center of mass is not aligned with the exact center of the target object.

Bennett et. al. used MSM to calculate the torque on a 3×1 m target cylinder due to a spherical tug craft for different voltages and angles [4]. This set up is shown in Fig. 5. The cylinder has the same voltage magnitude as the sphere, and is always positive while the tug sphere can change the polarity of its voltage: $V_2 = |\phi|$, $V_1 = \phi$. The torque is only about the z axis due to the symmetry, and is shown as a function of both the angle θ and the voltage ϕ. This plot is shown for near field (2.5 m separation) and far field (15 m separation) cases in Fig. 6. The voltage dependance follows a quadratic relationship, and the angular dependance is well approximated by $\sin(2\theta)$. The torque is then curve fit to be [4]:

$$L = \gamma f(\phi) g(\theta) = \gamma \phi |\phi| \sin(2\theta) \tag{61}$$

In the near field, γ divides into a larger value for attraction γ_a and a smaller value for repulsion γ_r. At further separations the difference between attraction and repulsion is less evident.

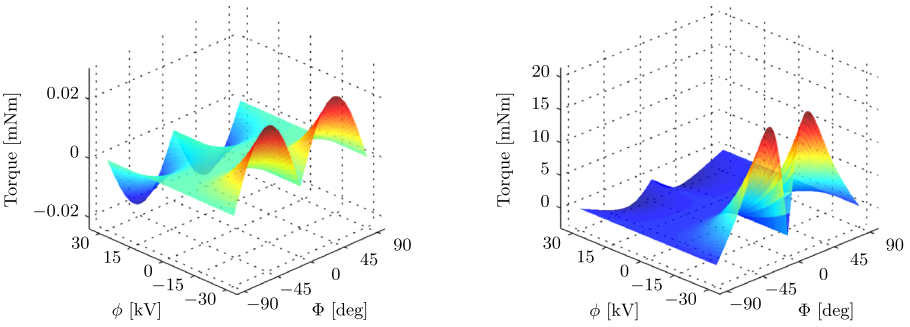

(a) Separation $d = 15$ m (b) Separation $d = 2.5$ m

Fig. 6 MSM torque surfaces at a separation distances of $d = 2.5$ m and $d = 15$ m for $V_1 = \phi$ and $V_2 = |\phi|$ [4]

The angular, voltage, and attraction/repulsion trends that have been empirically found using MSM are now derived using AFMs. Referencing Eq. 26, the torque on a general body due to a nearby point charge is given by

$$\boldsymbol{L}_2 = \frac{Q_1}{4\pi\epsilon_0 R_c^3}\left[\boldsymbol{q}_2 + \frac{3}{R_c^2}[Q_2]\boldsymbol{R}_c\right] \times \boldsymbol{R}_c \tag{62}$$

re-writing this in terms of susceptibilities gives:

$$\boldsymbol{L}_2 = \frac{C_{S1}V_1 + C_M V_2}{4\pi\epsilon_0 R_c^3}\left[\left(\boldsymbol{\chi}_S + \frac{3}{R_c^2}[\psi_S]\boldsymbol{R}_c\right)V_2 + \left(\boldsymbol{\chi}_M + \frac{3}{R_c^2}[\psi_M]\boldsymbol{R}_c\right)V_1\right] \times \boldsymbol{R}_c \tag{63}$$

This equation is grouped into four separate terms

$$\begin{aligned}\boldsymbol{L}_2 = \frac{1}{4\pi\epsilon_0 R_c^3}\Bigg[&C_M\left(\boldsymbol{\chi}_S + \frac{3}{R_c^2}[\psi_S]\boldsymbol{R}_c\right)V_2^2 + C_{S1}\left(\boldsymbol{\chi}_M + \frac{3}{R_c^2}[\psi_M]\boldsymbol{R}_c\right)V_1^2 \\ &+ \left(C_{S1}\left(\boldsymbol{\chi}_S + \frac{3}{R_c^2}[\psi_S]\boldsymbol{R}_c\right) + C_M\left(\boldsymbol{\chi}_M + \frac{3}{R_c^2}[\psi_M]\boldsymbol{R}_c\right)\right)V_1V_2\Bigg] \times \boldsymbol{R}_c \\ = \boldsymbol{A}V_1^2 + \boldsymbol{B}V_2^2 &+ (\boldsymbol{C} + \boldsymbol{D})V_1V_2\end{aligned} \tag{64}$$

In this 1-D case the torque is purely about the z axis and is written using scalars as

$$L = AV_1^2 + BV_2^2 + (C + D)V_1V_2 \tag{65}$$

The terms A and B have one mutual term and are thus 1st order in $(1/R_c)$, C is 0th order, and D is 2nd order. This means that in the far field terms linked to C will persist longer than those linked to A and B, which will persist longer than those linked to D. Because the mutual susceptibilities (C_M, $\boldsymbol{\chi}_M$, $[\psi_M]$) are negative but the self susceptibilities are positive, A, B and D are negative, but C is positive and larger than D.

Thus the following development switches to the positive variables $F = |A + B|$ and $G = C + D$, and makes use of the definitions $V_1 = \phi$, $V_2 = |\phi|$ to match prior work [4]. The torque for attractive (L_a) and repulsive (L_r) cases is given by:

$$L_r = (-F + G)\phi^2 = (-F + G)\phi|\phi| \tag{66}$$

$$L_a = (-F - G)\phi^2 = (F + G)\phi|\phi| \tag{67}$$

In the attractive cases the magnitude of the torque is larger because F and G add rather than subtract. This can be seen empirically in Fig. 6a. Additionally, since G has the highest order term, it will matter most in the far field. Since F matters less in the far field, the difference between the attractive and repulsive torque decreases in the far field, which can also be seen by comparing Fig. 6a and b.

In prior work Reference [4] numerically fit the far field parameter γ to a value of $2.234 * 10^{-14}$ for a 3 m by 1 m cylinder 15 m away from a 1 m diameter sphere. To compute the corresponding value from AFMs, assume that the center of mass is perfectly aligned with the center of charge so that $\boldsymbol{\chi}_S = 0$ and the body axes are aligned so that $[\psi_S]$ is given by $\text{diag}(\psi_B, \psi_s, \psi_B)$, where $\psi_B > \psi_s$. This represents the case of a perfectly axis-symmetric cylinder as shown in Fig. 5. Ignoring the mutual part of G which decays quickly gives the torque as

$$\begin{aligned} L &= \frac{-3C_{S1}}{4\pi\epsilon_0 R_c^5} \tilde{\boldsymbol{R}}_c [\psi_S] \boldsymbol{R}_c V_1 V_2 \\ &= \frac{3C_{S1}}{8\pi\epsilon_0 R_c^3} (\psi_B - \psi_s) \sin(2\theta) V_1 V_2 \hat{\boldsymbol{z}} \end{aligned} \tag{68}$$

where G is defined as

$$G = \frac{3C_{S1}}{8\pi\epsilon_0 R_c^3} (\psi_B - \psi_s) \tag{69}$$

SMSM is used to find the values of ψ_S and ψ_B which gives $G \approx 2.531 * 10^{-14}$, only a 13% difference with the numerically fit value used in Reference [4]. These two results agree well considering that only a second order AFM model is used and the mutual part of G is ignored, and Reference [4] fits γ to the full MSM solution.

Now consider the same cylinder, but allow the center of mass to move within the craft by a few centimeters along the y axis ($\boldsymbol{\chi}_S = [0, \chi_S, 0]^T$). The torque is still only about the z axis and is given by

$$\begin{aligned} \boldsymbol{L}_2 &= \frac{-C_{S1}}{4\pi\epsilon_0 R_c^3} \tilde{\boldsymbol{R}}_c \left(\boldsymbol{\chi}_S + \frac{3}{R_c^2} [\psi_S] \boldsymbol{R}_c \right) V_1 V_2 \\ &= \frac{-C_{S1}}{8\pi\epsilon_0 R_c^2} \left[\chi_S \cos(\theta) + \frac{3(\psi_B - \psi_s)}{2R_c} \sin(2\theta) \right] V_1 V_2 \hat{\boldsymbol{z}} \end{aligned} \tag{70}$$

Setting $\chi_S = 0$ recovers Eq. 68, but even a small CM offset can make the $\cos(\theta)$ term dominate, especially at large separations. As the CM moves away from the geometric center, χ_S grows linearly, and some elements of ψ_S grow quadratically. The torque as a function of θ is shown for a variety of CM offsets in the example of the same cylinder 15 m away from a 1 μC point charge in Fig. 7. The different curves are for different values of χ_S – the center of mass offset is shown in the legend.

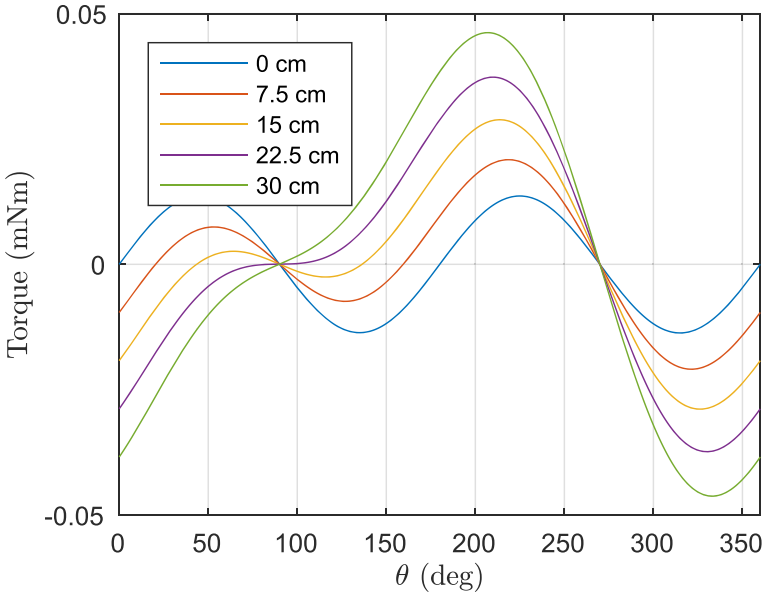

Fig. 7 Torque on cylinder for a variety of center of mass offsets

The torque slowly changes from a perfect $\sin(2\theta)$ to an augmented -$\cos(\theta)$ curve as the CM offset varies. The magnitude of the torque also increases by a factor of 3.38. This factor is even greater at further separations since the $\cos(\theta)$ term has lower order in $1/R_c$. Knowledge of center of mass to center of charge differences are essential for the stability of control laws used for de-spinning of passive space debris. If the center of charge location is not properly accounted for, the sign of the predicted torque can be wrong, leading to instabilities in the closed-loop control discussed in Reference [4].

Conclusion

This paper presents a novel method for analytically predicting the force and torque on conducting bodies using knowledge of the voltage of each, their relative separation, and relative attitude. This is accomplished by approximating the force and torque using a truncated binomial series to identify the first three moments of the charge distribution ($Q, \boldsymbol{q}, [Q]$). Next, these measures of the charge distribution are predicted using a capacitance-matrix formulation, where the structure of the capacitance matrix is found using MSM and the block pseudo inverse formula is approximated. This method yields less than 5% accuracy errors for separations larger than 50 m for the case of two 8 m template GEO satellites. This level of accuracy is sufficient for controls analysis beyond a few craft diameters.

The biggest strength of the AFMs is their ability to provide analytical force and torque expression for many control and dynamics applications. As an example, AFMs

are used to predict the torque on a cylinder in the presence of a nearby point charge. The sign and magnitude of the torque have a strong dependance on the possible offset between the center of mass and center of charge in the cylinder. While challenging to derive, AFMs offer analytic insight to difficult charged dynamics and control problems.

References

1. Bauer, R.: Distribution of points on a sphere with application to star catalogs. J. Guid. Control. Dyn. **23**(1), 130–137 (2000)
2. Bengtson, M., Wilson, K., Hughes, J., Schaub, H.: Survey of the electrostatic tractor research for reorbiting passive geo space objects. Astrodynamics. https://doi.org/10.1007/s42064-018-0030-0. (2018)
3. Bennett, T., Schaub, H.: Touchless electrostatic three-dimensional detumbling of large geo debris. In: AAS/AIAA Spaceflight Mechanics Meeting (2014)
4. Bennett, T., Schaub, H.: Touchless electrostatic three-dimensional detumbling of large axi-symmetric debris. J. Astronaut. Sci. **62**(3), 233–253 (2015)
5. Bennett, T., Schaub, H.: Capitalizing on relative motion in electrostatic detumbling of axi-symmetric geo objects. In: 6Th International Conference on Astrodynamics Tools and Techniques (ICATT). Darmstadt, Germany (2016)
6. Bennett, T., Stevenson, D., Hogan, E., McManus, L., Schaub, H.: Prospects and challenges of touchless debris despinning using electrostatics. Adv. Space Res. **56**(3), 557–568 (2015)
7. Berryman, J., Schaub, H.: Analytical charge analysis for 2- and 3-craft coulomb formations. AIAA Journal of Guidance, Control, and Dynamics **30**(6), 1701–1710 (2007)
8. Chow, P., Hughes, J., Bennett, T., Schaub, H.: Automated sphere geometry optimization for the volume multi-sphere method. In: AAS/AIAA Spaceflight Mechanics Meeting (2016)
9. Fennell, J., Koons, H., Leung, M., Mizera, P.: A review of scatha satellite results: charging and discharging. Tech. Rep. TR-0084a(5940-05)-7, The Aerospace Corporation, El Segundo CA (1983)
10. Früh, C., Ferguson, D., Lin, C., Jah, M.: The effect of passive electrostatic charging on near-geosynchronous high area-to-mass ratio objects. In: Proc. AAS Space Flight Mechanics Meeting. Santa Fe, NM, pp. 3121–3137 (2014)
11. Giancoli, D.C.: Physics for Scientists and Engineers. Pearson Prentice Hall, New Jersey (2008)
12. Gibson, W.C.: The Method of Moments in Electromagnetics. Chapman & Hall, London (2007)
13. Grafarend, E., Engles, J., Varga, P.: The temporal variation of the spherical and cartesian multipoles of the gravity field: the generalized maccullagh representation. J. Geod. (2000)
14. Griffiths, D.J. Introduction to Electrodynamics, 3rd edn. Prentice Hall, Englewood Cliffs (1999)
15. Harrington, R.: Field Computation by Moment Methods. Wiley IEEE, New York (1968)
16. Hogan, E., Schaub, H.: Collinear invariant shapes for three-craft coulomb formations. Acta Astronaut. **12**, 78–89 (2012). https://doi.org/10.1016/j.actaastro.2011.10.020
17. Hogan, E., Schaub, H.: Relative motion control for two-spacecraft electrostatic orbit corrections. AIAA Journal of Guidance, Control, and Dynamics **36**(1), 240–249 (2013)
18. Hou, X., Scheeres, D.J., Xin, X.: Mutual potential between two rigid bodies with arbitrary shapes and mass distributions. Celest. Mech. Dyn. Astron. **127**, 1–27 (2016)
19. Hughes, J., Schaub, H.: Appropriate fidelity electrostatic force evaluation considering a range of spacecraft separations. In: AAS/AIAA Spaceflight Mechanics Meeting (2016)
20. Hughes, J., Schaub, H.: Charged Geosynchronous Debris Perturbation Using Rapid Electromagnetic Force and Torque Evaluation Advanced Maui Optical and Space Surveillance Technologies Conference 86 (2016)
21. Hughes, J., Schaub, H.: Rapid charged geosynchronous debris perturbation modeling of electrodynamic disturbances. J. Astronaut. Sci. **65**(2), 135–156 (2018)

22. Hughes, J., Schaub, H.: Space weather influence on electromagnetic geosynchronous debris perturbations using statistical fluxes. AGU Space Weather **16**(4), 391–405 (2018). https://doi.org/10.1002/2017sw001768
23. Inampudi, R., Schaub, H.: Optimal reconfigurations of two-craft coulomb formation in circular orbits. AIAA Journal of Guidance, Control, and Dynamics **35**(6), 1805–1815 (2012)
24. Ingram, G., Hughes, J., Bennett, T., Reilly, C., Schaub, H.: Volume multi-sphere-model development using electric field matching. J. Astronaut. Sci. **65**(4), 377–399 (2018)
25. Jackson, J.D.: Classical Electrodynamics. Wiley, New York (1999)
26. King, L.B., Parker, G.G., Deshmukh, S., Chong, J.H.: Spacecraft formation-flying using inter-vehicle coulomb forces. Tech. rep., NASA/NIAC (2002)
27. King, L.B., Parker, G.G., Deshmukh, S., Chong, J.H.: Study of interspacecraft coulomb forces and implications for formation flying. AIAA Journal of Propulsion and Power **19**(3), 497–505 (2003)
28. Lekner, J.: Electrostatics of two charged conducting spheres. Procedings of the Royal Society **468**, 2829–2848 (2012)
29. Maxwell, J.: A treatise on electricity and magnetism. Oxford University Press, London (1893)
30. Paul, S.N., Früh, C.: Space debris charging and its effect on orbit evolution. Journal of Guidance, Control, and Dynamics **0**, 1–19 (2017)
31. Price, S., Stone, A., Alderton, M.: Explicit formulae for the electrostatic energy, forces and torques between a pair of molecules of arbitrary symmetry. Mol. Phys. **52**(4), 987–1001 (1984)
32. Schaub, H., Junkins, J.L.: Analytical Mechanics of Space Systems, 2nd edn. AIAA Education Series, Reston, VA (2009)
33. Schaub, H., Moorer, D.F.: Geosynchronous large debris reorbiter: challenges and prospects. J. Astronaut. Sci. **59**(1–2), 161–176 (2014)
34. Scheeres, D.J.: Orbital motion in strongly perturbed environments. Springer, Berlin (2012)
35. Smythe, W.R. Static and Dynamic Electricity, 3rd edn. McGraw–Hill, New York (1968)
36. Stevenson, D., Schaub, H.: Multi sphere modeling for electrostatic forces on three-dimensional spacecraft shapes. In: AAS/AIAA Spaceflight Mechanics Meeting. Charleston, South Carolina (2012)
37. Stevenson, D., Schaub, H.: Multi-sphere method for modeling electrostatic forces and torques. Adv. Space Res. **51**(1), 10–20 (2013). https://doi.org/10.1016/j.asr.2012.08.014
38. Stevenson, D., Schaub, H.: Optimization of sphere population for electrostatic multi sphere model. IEEE Trans. Plasma Sci. (2013)